A Double-Wiebe Function for Reactivity Controlled Compression Ignition Combustion Using Reformate Diesel

Ruinan Yang
Department of Mechanical Engineering,
Stony Brook University,
Stony Brook, NY 11794
e-mail: ruinan.yang@stonybrook.edu

Zhongnan Ran
Department of Mechanical Engineering,
Stony Brook University,
Stony Brook, NY 11794
e-mail: zhongnan.ran@stonybrook.edu

Rodrigo Ristow Hadlich
Department of Mechanical Engineering,
Stony Brook University,
Stony Brook, NY 11794
e-mail: rodrigo.ristowhadlich@stonybrook.edu

Dimitris Assanis[1]
Department of Mechanical Engineering;
Institute for Advanced Computational Science;
Advanced Energy Research & Technology Center,
Stony Brook University,
Stony Brook, NY 11794
e-mail: dimitris.assanis@stonybrook.edu

Reactivity controlled compression ignition (RCCI) combustion has previously been proposed as a method to achieve high fuel conversion efficiency and reduce engine emissions. A single-fuel RCCI combustion strategy can have decreased fuel system complexity by using a reformate fuel for port fuel injection and the parent fuel (diesel) for direct injection. This paper presents a one-dimensional computational model of a compression ignition engine with single-fuel RCCI. A Wiebe function is used to predict the combustion process by representing the mass fraction burned (MFB) on a crank angle resolved basis. One single-Wiebe function (SWF) and two double-Wiebe functions(DWFs) were fitted to experimentally derive MFB data using the least-square method. The fitted results were compared with MFBs calculated from experimental data to verify the accuracy. The SWF did not fully capture the MFB curve with high fidelity while the detailed DWF captured the MFB curve within a root mean square error of 1.4%. The reduced double-Wiebe function (RDWF) also resulted in a predicted combustion profile with similar accuracy. Hence, the RDWF was used in a GT-power thermodynamic study to understand the effects of the low-temperature heat release (LTHR) fraction and combustion phasing on combustion characteristics. At optimum phasing of 5–10 crank angle degree after the top dead center, increasing the LTHR fraction from 20% to 60% resulted in the fuel conversion efficiency increasing from 39.5% to 41.1%, thus suggesting that the reformate fuel-based RCCI strategy is viable to unlock improved combustion performance. [DOI: 10.1115/1.4053981]

Keywords: energy conversion/systems, energy systems analysis, combustion modeling, reformate diesel fuel, reactivity controlled compression ignition

1 Introduction

Internal combustion engines (ICEs) have been widely employed in power generation and transportation applications since the 20th century. In the quest to achieve higher fuel conversion efficiency, compression ignition (CI) engines are often favored to spark ignition (SI) engines. However, combustion with diesel engines also causes high exhaust emissions including carbon monoxide (CO), nitrogen oxides (NOx), particulate matter (PM), and unburned hydrocarbons (UHCs). Therefore, there exists a need for researchers to investigate different combustion strategies to achieve cleaner combustion while maintaining high enough efficiencies. Recently, researchers have been working on investigating better combustion modes that can accomplish the target and eliminate the disadvantages of CI combustion associated with harmful emissions [1].

Low-temperature combustion (LTC) strategies have been previously proposed as a pathway to meet emissions regulations that are required by government agencies, while still achieving comparable thermal efficiencies. Among all of the LTC strategies, homogeneous charge compression ignition (HCCI) is a promising strategy that unlocks near constant volume combustion. It can be achieved when fuel and air are premixed homogeneously during the intake stroke and subsequently compressed by the piston in the compression stroke to the point where auto-ignition occurs in the combustion chamber. HCCI combustion was first researched during the late 1970s by Noguchi et al. [2] and has since been experimented with various types of engines, fuels, and operating conditions in the past 30 years. Onishi et al. [3] proved that HCCI combustion could be performed easily on a two-stroke engine, and Najt and Foster [4] showed that it could be used on a four-stroke engine. Experimental results from past researchers like Kimura et al. [5] and Zhao et al. [6] showed that the HCCI combustion strategy emits less NOx and soot emissions than both SI and CI combustion and maintains similar efficiency compared with CI engines. However, although HCCI combustion can achieve the goal of emissions reduction, this combustion strategy is not currently being used in modern engines. Direct control of HCCI combustion remains challenging as it is governed by chemical kinetic reaction rates, thus making control of combustion phasing and heat release rates not readily achievable [7,8]. Meanwhile, the emissions of carbon monoxide and unburned hydrocarbons remain high.

In the meantime, several scientists also worked on LTC with advanced engine development technologies. The effect of piston bowl diameter was emphasized by Genzale et al. [9], and the results proved that the combustion chamber affected the fuel–air mixture and emissions. Bobba et al. [10] investigated the effect of post-injection on engine performance and showed that post-injection timing played a major role in combustion rather than the gap between the post and main injection. Cao et al. [11] computationally analyzed the relationship between injection timing, chamber geometry, and emissions. In this research, the vertical sidewall bowl was affirmed to achieve the lowest emissions.

[1]Corresponding author.

Contributed by the Internal Combustion Engine Division of ASME for publication in the Journal of Energy Resources Technology. Manuscript received September 23, 2021; final manuscript received February 22, 2022; published online April 11, 2022. Assoc. Editor: Yu Zhang.

Past LTC research by Bessonette et al. [12] has shown that fuels with auto-ignition qualities spanning from gasoline to diesel fuels can be suitable to be used in HCCI combustion. Inagaki et al. [13] demonstrated a combustion mode that utilized a premixed low cetane number fuel and a subsequent high cetane number fuel that was directly injected. Meanwhile, Kokjohn et al. [14] also showed that dual-fuel combustion mode, reactivity controlled compression ignition (RCCI) combustion, is a possible pathway to achieve increased control of the combustion process. Specifically, RCCI is a dual-fuel combustion mode that utilizes chemical reactivity differences in the two fuels to control the combustion phasing, duration, and magnitude of the combustion process. Experimental research conducted by Dempsey et al. [15] explored various dual-fuel low-temperature combustion modes, including dual-fuel HCCI, dual-fuel premixed charge compression ignition, single-fuel partially premixed combustion, and dual-fuel RCCI, and compared their combustion controllability, combustion sensitivity to intake conditions and emissions. Kokjohn et al. [16] experimentally demonstrated dual-fuel RCCI combustion using gasoline and diesel fuels over a significant range of engine loads, all while achieving high fuel conversion efficiency and low NOx and PM emissions. Hanson et al. [17] also investigated RCCI combustion controllability by varying fuel injection timing and quantities. Ryan Walker et al. [18] experimentally investigated methane/diesel RCCI combustion and proved that the engine operating envelope could be expanded in comparison to RCCI combustion with gasoline and diesel as the fuels. Additionally, Reitz and Duraisamy as well as Paykani et al. have extensively reviewed the literature to show that RCCI is a potential low-temperature combustion strategy that achieves high efficiency and low emissions [19,20].

Since RCCI combustion ultimately needs two fuels, featuring different reactivities, to control the combustion process, it is anticipated that the fuel delivery and storage systems will increase in complexity. As an alternative, single-fuel RCCI combustion has been proposed in recent years. For example, one could add a cetane improver into the low reactivity fuel to effectively dope the fuel into behaving as a higher reactivity fuel. For this concept, part of the low reactivity fuel is injected at the intake port and premixed with air, while the rest of the fuel is mixed with improvers such as di-tert butyl peroxide (DTBP) [21] and 2-ethylhexyl nitrate [22,23] and injected into the cylinder directly. Splitter et al. [24] experimented using gasoline at intake port and gasoline doped with an improver in the cylinder to achieve single-fuel RCCI combustion. Results showed that a small amount of additive had an apparent effect on fuel reactivity and therefore satisfied the requirement of achieving fuel reactivity for RCCI combustion.

Fuel reforming has been proposed in recent decades as another strategy to accomplish single-fuel RCCI combustion mode. Lawler and Mamalis patented an onboard reformation process to accomplish this single-fuel RCCI strategy [25]. Chuahy and Kokjohn [26] illustrated a combustion mode using syngas as the low reactivity fuel and diesel as the high reactivity fuel. A type of green syngas relevant to modern power generation is anode-off gas, which is readily produced as a byproduct of solid oxide fuel cells. Ran et al. [27,28] and Nikiforakis et al. [29] demonstrated the feasibility of using anode-off gas as a primary fuel in internal combustion engines. Another interesting type of gaseous fuel is reformate which is generated by external catalytic reforming of liquid fuel. Hariharan et al. [30] and Yang et al. [31] presented a group of studies with two kinds of diesel reformate fuel generated by the catalytic partial oxidation process, which includes H_2, CO, and several partially oxidized hydrocarbons. The reactivities of the reformate fuels were determined by a research octane number map. This study showed that two reformate fuels resulted in low lower heating value (LHV) compared to conventional hydrocarbon fuels. Hariharan et al. [32] also quantified the combustion characteristics and emissions of single-fuel RCCI combustion with varying ignition timing and reformate-diesel blend ratio (BR) using the two reformate fuels.

In principle, most compression ignition engines are designed for use with commercial diesel fuels. Therefore, using reformate fuels in conventional diesel engines requires modifications to the engine injection system and operating conditions, and also intensive studies of utilizing single-fuel RCCI combustion strategies.

Computational modeling of the ICE combustion process is a critical part of the design, calibration, and understanding of advanced engine technologies [33]. Models of engine combustion are divided into two broad categories, zero-dimensional (0D), thermodynamic, energy-based and multidimensional, fluid dynamic-based models [34]. Thermodynamic models can be formulated as single zone or multi zone [35–37]. A single zone 0D model, based on the first law of thermodynamics, is often used in engine simulation studies due to its reduced requirement on computational time at the expense of model accuracy [35]. The input to such an efficient in-cylinder combustion model is the fraction of fuel mass burned during the combustion as a function of crank angle degrees (CADs).

The Wiebe function has extensively been used in engine modeling studies to determine mass fraction burned (MFB) combustion profile [34,38–40]. This normalized function generates an S-shaped MFB curve that ranges from the value of zero to one [41]. A value of zero corresponds to 0% of the MFB and delineates the start of combustion, while a value of one corresponds to 100% of the MFB and delineates the end of combustion. The standard single-Wiebe function (SWF) generally shows a high modeling accuracy for SI combustion engine simulations, while it has proved to be less reliable when used with advanced combustion modes [42,43]. On the other hand, a double-Wiebe function (DWF) was demonstrated by Yasar et al. [38] for HCCI combustion, where a second Wiebe function was proposed to capture boundary combustion conditions. The DWF is also generally used to capture the fraction of fuel burned for compression ignition, which includes premixed combustion and diffusion combustion. A modified DWF was introduced by Yeliana et al. [42] and was well validated with a SI combustion engine. Yıldız and Albayrak Çeper [44] generated a double function that was used to simulate the combustion process in a methane and methane-hydrogen blend SI engine. Liu and Dumitrescu [45] modified a DWF with a signum function to describe the MFB curve in a diesel engine. Liu and Dumitrescu [46] and Liu et al. [47] also introduced a triple Wiebe function to model the combustion of a spark ignition engine fueled with natural gas. Additionally, Awad et al. [48] introduced a triple Wiebe function to describe the combustion process and characteristics of a diesel engine fueled with biodiesel. Additionally, Yang et al. [49] have previously been successful at using a DWF to describe syngas/anode-off gas and diesel fuel under RCCI/dual-fuel combustion conditions.

In this paper, an SWF and two DWFs were developed and compared in their ability to predict the MFB profile of a single-fuel RCCI combustion mode, achieved by running diesel and reformate fuel in a CI engine. The Wiebe function corresponding coefficients were computed by performing a heat release analysis of the measured pressure data and using the least-square method for data-fitting. Subsequently, a one-dimensional (1D) system-level model was created and calibrated for further thermodynamic analysis. The fitted Wiebe functions were used to predict heat release rates, which were imported in the well-validated model to produce the modeling pressure traces. By comparing those profiles against experimental results, the accuracy and validity of the three Wiebe functions could then be examined. The equation with the highest accuracy and lowest complexity was selected for further studies of the heat release rates using a baseline case. In the following sections, a thermodynamic study and fundamental first law analysis are performed to understand the effects of low-temperature heat release (LTHR) fraction and combustion phasing on single-fuel RCCI combustion by determining MFB profiles that generate the highest efficiency. This study was performed to qualitatively analyze the effects of the combustion process and associated heat release on the fuel conversion efficiency performance. Determining such effects can allow for the optimization of the reformate fuel

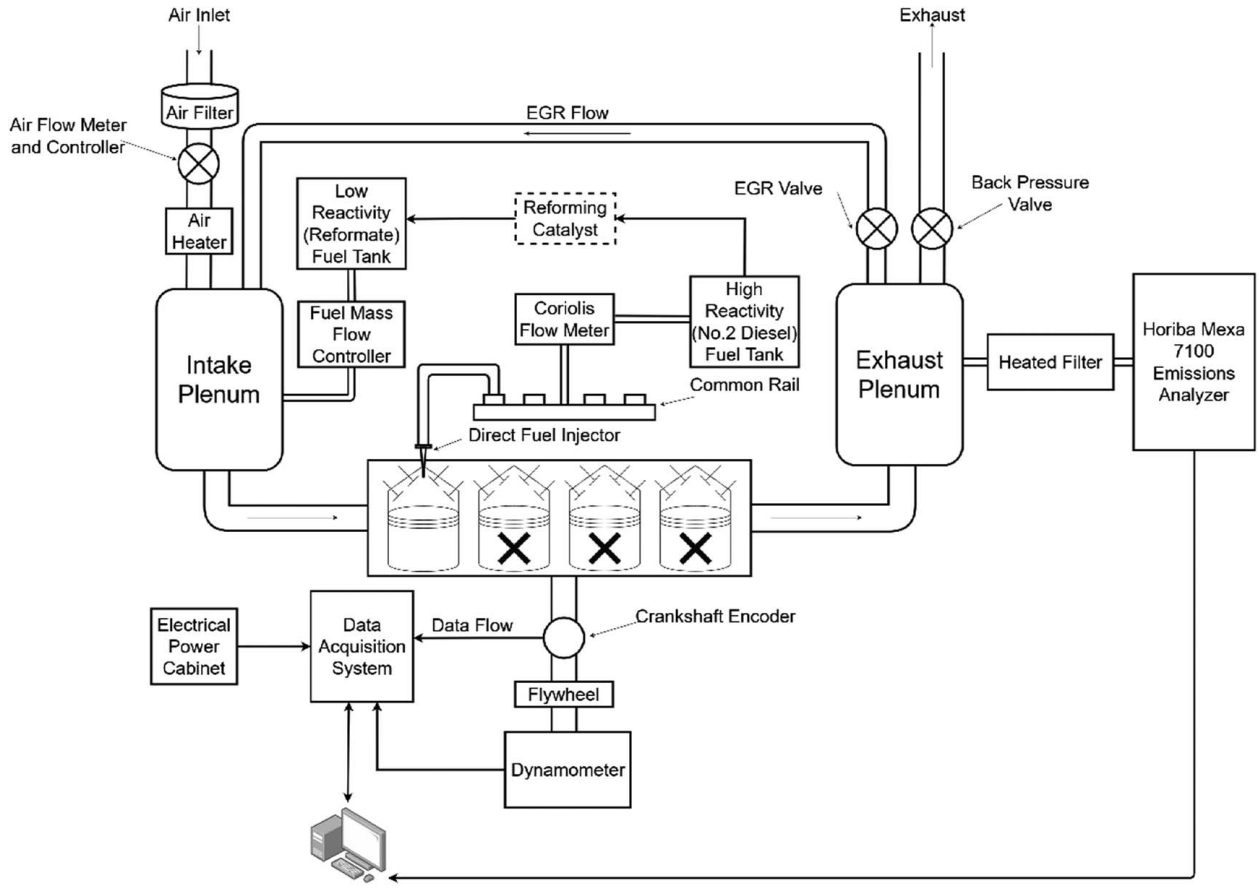

Fig. 1 The single-cylinder single-fuel RCCI experimental setup at Stony Brook University has been adapted from Ref. [50] for use in this study

catalyzing process to yield desirable fuel components and for the shift of engine operating conditions to achieve the most ideal single-fuel RCCI combustion possible.

2 Experimental Setup and Methodology

2.1 Experimental Setup. The experimental study was conducted on a 1.7 L four-cylinder General Motors diesel engine with a Ricardo Hydra research engine block. One cylinder is used for the experiments and the three remaining cylinders were deactivated. Figure 1 shows the engine setup schematic, while Table 1 shows the specifications of the engine.

Air at atmospheric pressure is inducted through an intake air filter. A compressor controlled by a pressure regulator is set next to the setup to supply dry boosted air to the engine. The intake airflow pressure and flowrate are measured and controlled by an Alicat airflow meter. The intake air is heated by a proportional-integral-derivative (PID) controlled intake heater, and an intake plenum downstream of the heater is used to reduce the pressure fluctuations. The fuel for the port fuel injection (PFI) and direct injection (DI) systems is supplied from a customized fuel cart located next to the engine. Two micro-motion Coriolis fuel flow meters are used to measure both the PFI and DI fuel flowrates. Gaseous fuel is supplied from compressed gas bottles into the intake plenum and premixed with intake air. The gaseous fuel pressures and fuel flowrates are controlled by an Alicat mass flow controller. Two PID-controlled heaters and radiators are used to control the coolant and oil temperatures.

Table 1 Ricardo Hydra single-cylinder engine specifications (further details can be found in Ref. [32])

Bore (mm)	79
Stroke (mm)	86
Connecting rod (mm)	160
Piston offset (mm)	0.6
Compression ratio	17
Optical encoder shaft resolution (CAD)	0.1
Intake valve opening (CAD aTDC)	−354
Intake valve closing (IVC) (CAD aTDC)	−146
Exhaust valve opening (CAD aTDC)	122
Exhaust valve closing (CAD aTDC)	366

Cylinder pressure, intake pressure, exhaust pressure, and common rail pressure are all measured and collected with Kistler high-speed pressure transducers. A Kistler optical shaft encoder with a resolution of 0.1 crank angle degree (CAD) is used to trigger the high-speed signal readings. The emission samples are measured and analyzed via a Horiba MEXA7100 D-EGR emissions bench. The data acquisition system is built based on two National Instruments CompactRio systems with an in-house built LABVIEW program for real-time data collection, post-processing, and engine operation controlling.

To achieve single-fuel RCCI, a reformate fuel mixture must be catalytically derived from the parent diesel fuel, which is used as the high reactivity fuel. The reformate fuel will serve as the secondary, low reactivity fuel. Further compositional and thermophysical property details of the diesel reformate fuel are provided in Table 2.

In this simulation study, 12 groups of experimental data were collected and analyzed from the single-fuel RCCI combustion. The operating conditions for the experiments were a fixed intake pressure of 1.4 bar, an intake temperature (T_{in}) sweep from 320 K to 350 K, and two different blend ratios of 35 and 50. The blend

Table 2 Diesel reformate fuel composition and related properties [32]

Acetylene (%)	0.05
Methane (%)	1.35
Ethylene (%)	2.90
Carbon dioxide (%)	11.09
Carbon monoxide (%)	3.40
Hydrogen (%)	3.07
Nitrogen (%)	79.15
Density (kg/m^3)	1.19
Lower heating value (MJ/kg)	2.32

ratio used during the experiments is determined with Eq. (1):

$$\text{BR} = \frac{\text{Energy of reformate fuel}}{\text{Total fuel energy}} \times 100\% \tag{1}$$

Heat release analysis, based on the first law of thermodynamics, was performed on the experimental data. The fuel–air charge mixture was considered an ideal gas. Heat loss from the valve, blowby, conduction heat transfer, and radiation heat transfer was neglected. The apparent heat release rate can thus be calculated using Eq. (2):

$$\frac{dQ}{d\theta} = \frac{\gamma}{\gamma - 1} p \frac{dV}{d\theta} + \frac{1}{\gamma - 1} V \frac{dp}{d\theta} + \frac{Q_{\text{heat}}}{d\theta} \tag{2}$$

where Q, θ, γ, p, V, and Q_{heat} refer to the heat release rate, crank angle, ratio of specific heat, cylinder pressure, combustion chamber volume, and heat transfer to the wall, respectively. The cylinder pressure was measured as a function of crank angle and the ratio of specific heats was defined from the composition of the mixture, the instantaneous temperature, and the instantaneous pressure. The volume was calculated based on the crank angle and geometry. The heat transfer to the wall was conducted by Eq. (3):

$$\frac{Q_{\text{heat}}}{dt} = hA(T - T_{\text{wall}}) \tag{3}$$

where h, A, T, and T_{wall} represent the heat transfer coefficient, combustion chamber surface area, instantaneous temperature, and wall temperature, respectively. In Eq. (3), the heat transfer coefficient was defined by the Hohenberg heat transfer correlation [51]:

$$h = a_s V(\theta)^{-0.06} p(\theta)^{0.8} T(\theta)^{-0.4} (S_p + b)^{0.8} \tag{4}$$

where S_p refers to mean piston speed while a_s and b are constants with values 130 and 1.4, respectively. The MFB was calculated based on the cumulative heat release during the combustion and will serve as an input to the 1D combustion model. The engine is considered a steady-state, and the energy balance for a cycle is defined by Eq. (5):

$$\dot{Q}_f = \dot{W}_n + \dot{Q}_e + \dot{Q}_h \tag{5}$$

where $\dot{Q}_f$ is the fuel energy rate, $\dot{W}_n$ is the net work, and $\dot{Q}_e$ is the exhaust energy rate. The fuel input energy into the control volume can be obtained from Eq. (6):

$$\dot{Q}_f = \dot{m}_f \text{LHV} \tag{6}$$

where $\dot{m}_f$ is the fuel flowrate and LHV is the lower heat value of the fuel. The net work can be divided into two parts, which is shown in Eq. (7):

$$\dot{W}_n = \dot{W}_g + \dot{W}_p \tag{7}$$

where $\dot{W}_g$ is the gross work and $\dot{W}_p$ is the pumping work. The exhaust energy rate is calculated by Eq. (8):

$$\dot{Q}_e = \dot{m}_e C_{p\_\text{exh}} T_{\text{exh}} \tag{8}$$

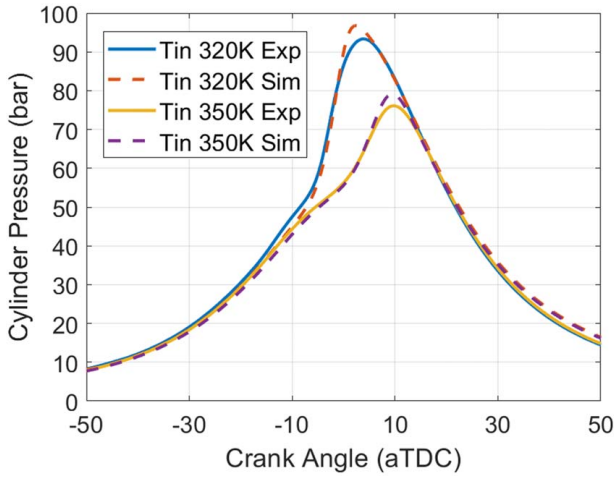

Fig. 2 Calibrated numerical model results in good agreement with corresponding experimental conditions

2.2 Simulation Model. In this paper, a system-level commercial software (Gamma Technologies GT-POWER) was employed for the engine simulation of the single-fuel RCCI combustion mode. Further details of this software and model theory details can be found in the GT-POWER user manual guide [52]. The intake and exhaust pipes used the 1D Navier–Stokes equation to calculate the flow and mechanical properties. The intake and exhaust valve lift profiles were measured and generated from the experimental setup. The 1D combustion model used the Combprofile function, and a normalized cumulative gross heat release calculated from the experimental results was used to calibrate the model. The model used the Hohenberg heat transfer correlation to capture heat loss to the wall. Figure 2 illustrates the comparison between experimental and computational results. Two experimental cases with intake temperatures at 320 K and 350 K are shown in the figure. Exp refers to experimental data and Sim refers to the simulation result. As can be seen from the figure, the cylinder pressure generated from the model was well validated against measured cylinder pressure data.

2.3 Wiebe Function Combustion Model. The MFB curve during combustion represents the percentage of fuel involved in chemical reaction versus crank angle, as determined by dividing the cumulative energy released by the total energy input. A Wiebe function is proposed and used to predict the MFB curve.

The SWF is shown in Eq. (9) [34]:

$$x_b(\theta) = 1 - \exp\left[-a\left(\frac{\theta - \theta_0}{\Delta\theta}\right)^{m+1}\right] \tag{9}$$

where $x_b(\theta)$ is the percentage of total mass fraction burned, θ is the engine's crank angle with respect to top dead center (TDC), θ_0 is the crank angle corresponding to the start of the combustion, $\Delta\theta$ corresponds to the combustion duration in CAD, m is the form factor, and a is the efficiency parameter.

The DWF, originally intended to approximate the (1) premixed and (2) diffusion combustion mode experienced in compression ignition engines, combines two standard SWFs using a relative weighting factor. This has been demonstrated to sufficiently predict the fraction of fuel burned in both SI and HCCI combustion

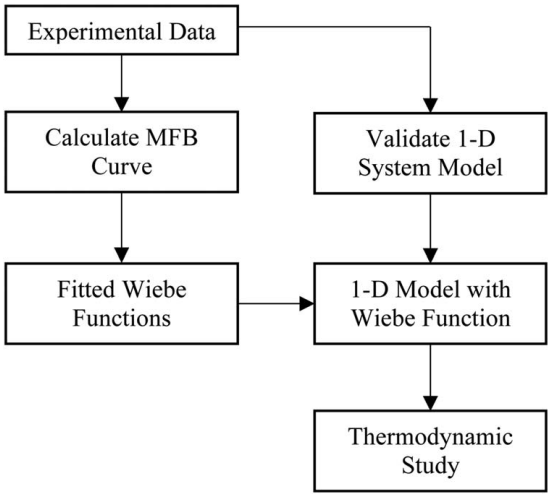

Fig. 3 Model flowchart

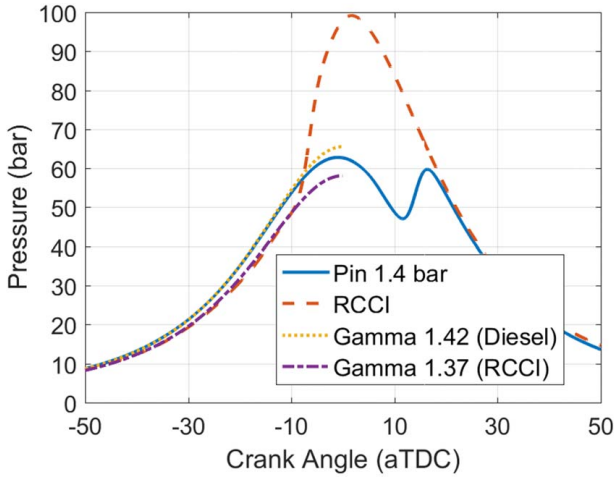

Fig. 4 In-cylinder pressure compared for traditional diesel combustion, RCCI combustion, and corresponding polytropic ideal cycles

modes. The form is expressed as Eq. (10) [44]:

$$x_b(\theta) = \lambda\left\{1 - \exp\left[-a_1\left(\frac{\theta-\theta_0}{\Delta\theta_1}\right)^{m_1+1}\right]\right\} + (1-\lambda)\left\{1 - \exp\left[-a_2\left(\frac{\theta-\theta_0}{\Delta\theta_2}\right)^{m_2+1}\right]\right\} \quad (10)$$

where λ is the weight factor and n stands for combustion stage n. In this study, this DWF in Eq. (10) is referred to as the detailed double-Wiebe function (DDWF).

If the efficiency factor, a, is defined as the same value, the DDWF can be defined by Eq. (11):

$$x_b(\theta) = \lambda\left\{1 - \exp\left[-a\left(\frac{\theta-\theta_0}{\Delta\theta_1}\right)^{m_1+1}\right]\right\} + (1-\lambda)\left\{1 - \exp\left[-a\left(\frac{\theta-\theta_0}{\Delta\theta_2}\right)^{m_2+1}\right]\right\} \quad (11)$$

Compared with Eq. (10), this modified form resulted in an improvement in reducing the complexity of the equation. In this study, this DWF is referred to as the reduced double-Wiebe function (RDWF).

The Wiebe function coefficients were determined using experimental data by fitting the normalized cumulative heat release data using the least-square method. The accuracy of the predicted MFB profile is evaluated by the value of the root-mean-square error (RMSE) between experimental data and the estimated function, which is calculated by Eq. (12):

$$\text{RMSE} = \sqrt{\frac{1}{i}\sum_{1}^{i}(y_p - y_r)^2} \quad (12)$$

where i is the number of data, y_p is the predicted value, and y_r is the regression's dependent value. After estimating the coefficients, a 1D engine system modeling study is performed to estimate the combustion process in the cylinder using the 0D model mentioned in Sec. 2.2. The stages of this simulation study are shown in Fig. 3.

3 Results and Discussion

Figure 4 illustrates the cylinder pressure traces for both conventional diesel and RCCI combustion modes with the same equivalence ratio and intake pressure. The average ratio of specific heats (γ) of the charge mixture during compression is 1.42 for diesel combustion and 1.37 for RCCI combustion, all at an intake pressure of 1.4 bar. As can be seen, the peak pressure achieved under RCCI combustion is significantly higher than that of diesel combustion. This indicates that the RCCI combustion has a wider range of peak pressure rise rates than conventional compression ignition under the same threshold of ringing intensity, which means that single-fuel RCCI combustion can extend this operating range limitation and potentially achieve a higher load, as shown in previous research by Wang et al. [53]. The figure also shows the simulated pressures during the compression stroke of two polytropic cycles

Table 3 Detailed parameters for the numerical single-Wiebe and double-Wiebe functions

		Single-Wiebe function (SWF)		Detailed double-Wiebe function (DDWF)					Reduced double-Wiebe function (RDWF)			
Intake temperature (K)	Blend ratio (%)	a	m	λ	a_1	m_1	a_2	m_2	λ	a_1	m	a_2
340	35	12.18	0.89	0.57	11.78	8.35	3.55	0.78	0.57	3.02	8.34	0.78
340	35	12.8	0.97	0.58	11.16	7.96	3.47	0.82	0.58	3.49	7.96	0.82
340	35	15.9	1.21	0.6	9.97	7.03	3.41	0.91	0.6	3.55	7.03	0.91
350	35	14.86	1.2	0.6	10.31	8.34	3.39	0.96	0.6	3.51	8.34	0.96
340	50	7.24	0.37	0.57	13.53	6.79	3.27	0.59	0.57	3.36	6.79	0.59
340	50	8.56	0.52	0.59	12.86	6.99	3.27	0.66	0.59	3.27	6.99	0.66
340	50	10.43	0.71	0.6	11.94	6.71	3.31	0.72	0.6	3.34	6.71	0.72
340	50	9.6	0.5	0.61	12.19	4.65	3.26	0.51	0.61	3.33	4.65	0.51
340	50	13	0.79	0.64	10.59	4.41	3.19	0.61	0.64	2.9	4.41	0.6

with γ and initial pressure taken from conventional diesel mixing controlled compression ignition combustion and RCCI combustion data at intake valve closing (IVC). The polytropic trace is close to experimental data with the same ratio of specific heats, which demonstrates that the difference in fuel properties is one of the main reasons for the misalignment in-cylinder pressure trace between diesel and single-fuel RCCI combustion at compression stroke.

3.1 Mass Fraction Burned. The normalized cumulative heat release profile was derived from experimentally collected cylinder pressure data and further processed to determine combustion performance metrics including phasing and duration. The MFB curve was then determined using curve fitting of the SWF parameters, a model intended to describe a singular stage of combustion, to determine the above combustion performance metrics. The start of combustion is defined as the CAD associated with 0% of the fuel burned, whereas the combustion duration is defined as the crank angle period between the start and end of the MFB curve. Among all 12 cases, nine groups of data were used as a training set to estimate the coefficients for all the functions, and the other three cases were used as validation data to evaluate the accuracy of the determined equation coefficients. An average of RMSE between experimental data and computational results was used to evaluate the fitting. Equation (13) shows the SWF, which minimizes the RMSE of the MFB curve to be 8.1%, and Table 3 shows the parameters for each case:

$$x_b(\theta) = 1 - \exp\left[-11.62\left(\frac{\theta - \theta_0}{\Delta\theta}\right)^{0.79+1}\right] \tag{13}$$

The DDWF and RDWF defined in Sec. 2.3 included two combustion stages. For the DDWF, the combustion phasing for stages one and two were assumed to be the same. The end of combustion for the primary stage was estimated by the least-square method, whereas for the secondary stage, it was defined as the ending CAD when all fuel had been consumed. Equation (14) shows the coefficients of the DDWF with a minimized RMSE of 1.4%, and Table 3 shows the coefficients for the function:

$$x_b(\theta) = 0.6\left\{1 - \exp\left[-11.59\left(\frac{\theta - \theta_0}{\Delta\theta_1}\right)^{6.8+1}\right]\right\} + (1 - 0.6)\left\{1 - \exp\left[-3.35\left(\frac{\theta - \theta_0}{\Delta\theta_2}\right)^{0.73+1}\right]\right\} \tag{14}$$

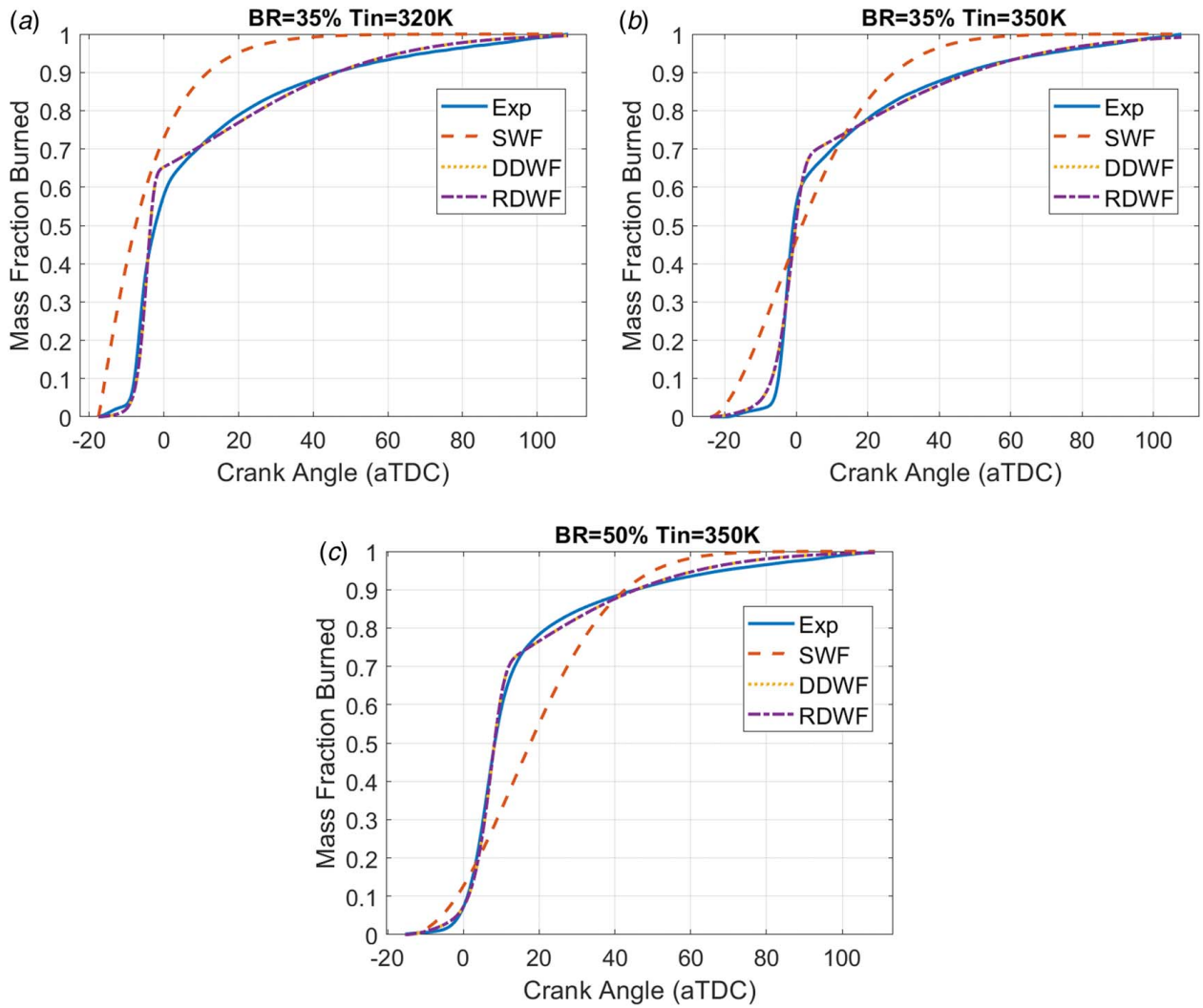

Fig. 5 MFB curves comparing the experimental and numerically predicted single-Wiebe and double-Wiebe functions shown for operating conditions consiting of: (*a*) blend ratio of 35% and intake temperature of 320 K, (*b*) blend ratio of 35% and intake temperature of 350 K, and (c) blend ratio of 50% and intake temperature of 350 K

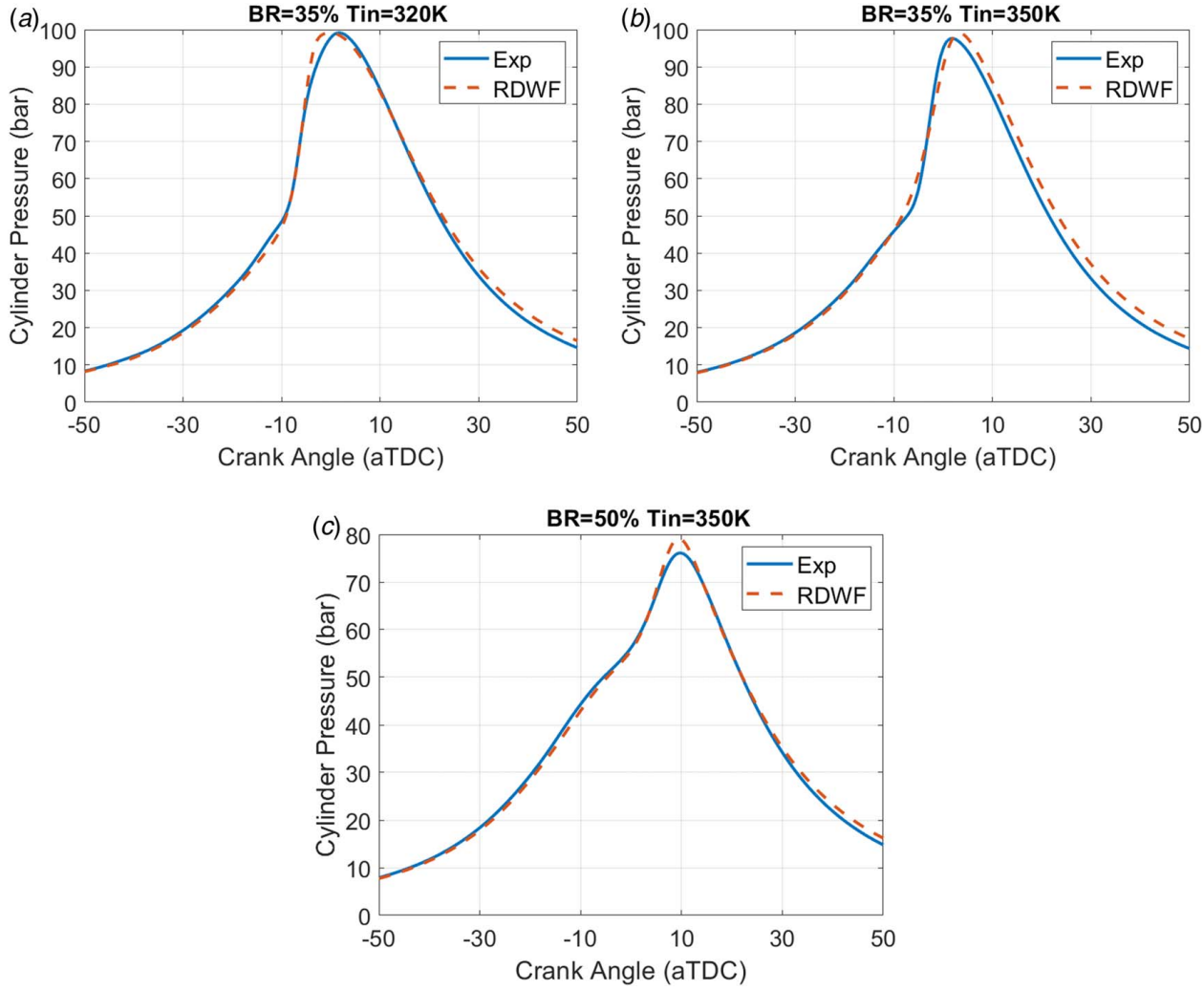

Fig. 6 Experimental and model-predicted pressure traces shown for shown for operating conditions consiting of: (*a*) blend ratio of 35% and intake temperature of 320 K, (*b*) blend ratio of 35% and intake temperature of 350 K, and (c) blend ratio of 50% and intake temperature of 350 K

Equation (15) illustrates the parameters with a minimized RMSE of 1.3%:

$$x_b(\theta) = 0.6\left\{1 - \exp\left[-3.31\left(\frac{\theta-\theta_0}{\Delta\theta_1}\right)^{6.8+1}\right]\right\} + (1-0.6)\left\{1 - \exp\left[-3.31\left(\frac{\theta-\theta_0}{\Delta\theta_2}\right)^{0.73+1}\right]\right\} \quad (15)$$

The coefficients for each case are shown in Table 3. Equations (14) and (15) resulted in the smallest average RMSE in contrast to the results of Eq. (13). The RMSE of Eq. (15) is similar to Eq. (14), which means that the RDWF with a reduced number of coefficients has similar accuracy as the DDWF. However, the RMSE of the SWF is much larger than the DWFs, which proves that the standard Wiebe function is not able to fully capture the combustion characteristics of the single-fuel RCCI combustion and hence is not suitable to predict the MFB curve.

Table 4 Operation condition and combustion characteristics of the baseline experiment

Intake temperature (K)	320
Blend ratio (%)	35
Combustion phasing (CAD aTDC)	−2.2
LTHR fraction (%)	2.5
Gross indicated mean effective pressure (kPa)	517.84
Indicated gross thermal efficiency (%)	33.52

Figure 5 compares the measured normalized cumulative heat release profile with the MFB curve predicted by the SWF and DWF for three selected cases that were not used in the curve fitting. The operating conditions for the three groups of data were (a) intake temperature at 320 K with a blend ratio of 35%, (b) intake temperature of 350 K and blend ratio of 35%, and (c) intake temperature of 350 K with a blend ratio of 50%, respectively. Exp refers to experimental data, SWF refers to a single-Wiebe function, DDWF refers to detailed double-Wiebe function, and RDWF refers to reduced double-Wiebe function.

It can be seen from Fig. 5 that the DDWF and RDWF of Eqs. (14) and (15) can accurately predict the combustion process of single-fuel RCCI combustion over a range of operating conditions. For the DDWF, the weight factor is determined as 0.6, which means the percentage of fuel burned in premixed combustion and diffusion combustion is close to each other. The form factor for stage one is much larger than stage two, which means stage one has a slower ignition, but faster flame propagation, while stage two has a faster ignition at the start of combustion, but a slower flame propagation.

Meanwhile, the initial small deviation from the horizontal line that can be discerned in both the experimental and simulated data shown

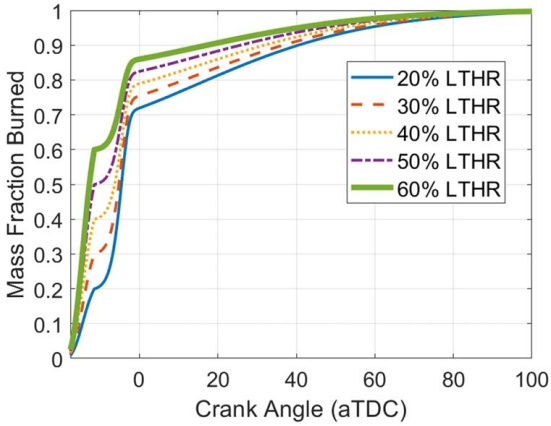

Fig. 7 MFB curves predicted by the double-Wiebe function and experimental data with varying LTHR fraction

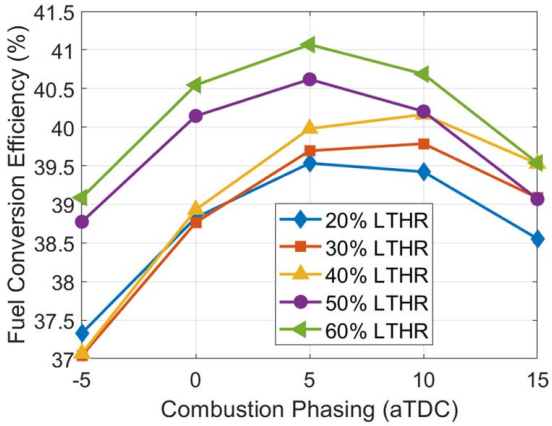

Fig. 10 Gross fuel conversion efficiency with respect to the combustion phasing at different LTHR fractions

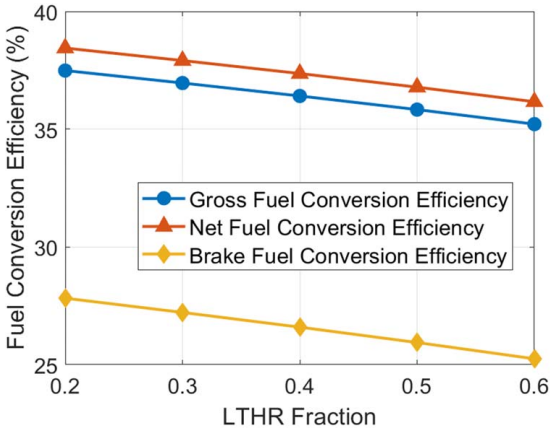

Fig. 8 Gross fuel conversion efficiency and brake fuel conversion efficiency with respect to the LTHR fraction

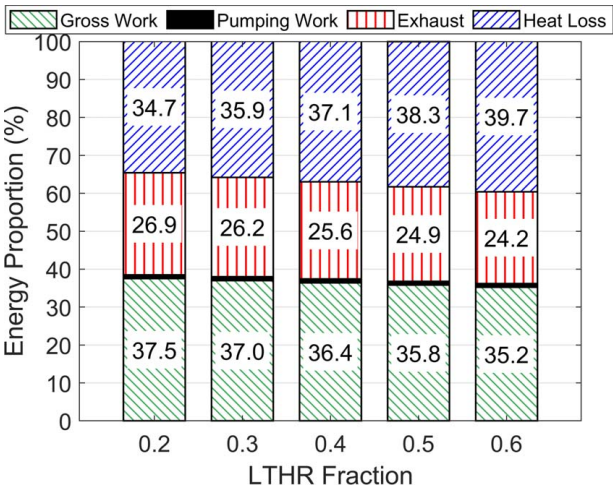

Fig. 9 Total engine system energy distribution with respect to the LTHR fraction

in Fig. 5 marks the beginning of the combustion process and is defined as the LTHR region, while the main heat release section is defined as high-temperature heat release (HTHR). Curve fitting the DWF to match the MFB profile during the LTHR region is quite difficult and thus local fidelity can be sacrificed to achieve global fidelity since the LTHR region here typically accounts for only 2–5% of the total heat release. The results of Eq. (15), in comparison to Eq. (14), achieve similar accuracy, within 0.1% RMSE, and are able to follow the trend of the experimental data, capturing most of the characteristics of RCCI combustion with less modeling complexity. On the other hand, the MFB curve generated from the standard Wiebe function is not able to capture the trend of experimental data, since the SWF has a standard exponential curve shape, which is different from the calculated profile.

Figure 6 portrays the experimental cylinder pressure data compared to the cylinder pressure data derived from simulated results that were reproduced using the RDWF. The cylinder pressure traces show a similar accuracy as observed in the MFB profile shown in Fig. 5, which proves that the RDWF can accurately fit experimentally derived MFB curves. It is worthy to note that there exists a small deviation in the pressure traces between experimental and simulated results at the top dead center (TDC). This stems from a small offset observed in the computationally determined MFB curves due to a small fraction of heat release occurring early in the compression stroke, which ultimately could not be captured by the DWF.

3.2 Low-Temperature Heat Release Fraction. The LTHR which appears in RCCI combustion was caused by diesel fuel and affected by the octane number of the low reactivity fuel. In order to better understand the relationship between LTHR and combustion characteristics, a study of LTHR fraction and combustion timing was performed. In this section, the relationship between the fraction of LTHR and engine performance is investigated. An initial set of experimental data was employed in the 1D model, under the operating conditions detailed in Table 4.

The predicted MFB curve from the RDWF was employed in the model. As mentioned in the previous section, the fitted curve is not able to fully capture the section of LTHR. To have a more precise result and a better understanding of the relationship between combustion process and engine performance, a MFB curve combining LTHR data from the experiments and HTHR data from the DWF was used in the model. The MFB profile was generated by varying the LTHR fraction from 20% to 60% and reducing the corresponding HTHR to reach the total normalized heat release to 100%. The starting crank angle and duration of the combustion event were maintained constant. The modified MFB curve is shown in Fig. 7.

Figure 8 shows the indicated gross fuel conversion efficiency and brake fuel conversion efficiency with respect to the LTHR fraction. Figure 9 illustrates the energy distribution with respect to the fraction of LTHR, by setting the total energy input constant for all cases. The fraction of pumping work for all cases is approximately 1%. In Fig. 8, both the indicated efficiency and brake efficiency are reduced from 38.4% to 36.2% and from 27.8% to 25.3%, respectively, as the LTHR fraction is increased from 0.2 to 0.6. The decrease in indicated efficiency is due to the increase in LTHR at

compression stroke, which results in a higher bulk temperature in the cylinder. A higher cylinder temperature increases the heat transfer coefficient, and thus increases the heat transfer loss to the cylinder wall, as shown in Fig. 9. Since more combustion occurs during the compression stroke, where the piston is moving in the opposite direction of the expanding fuel–air mixture, this causes an increase in compression work, which reduces the gross work, as shown in Fig. 9. A similar result was established by Splitter et al. [24] using gasoline and DTBP additive. The energy in the exhaust gas is reduced from 26.9% to 24.2%, and the heat loss is increased from 34.7% to 39.7%, with increases in the LTHR fraction. The combustion during the compression stroke also generates a higher amount of friction, which causes a decrease in torque and thus a decrease in brake fuel conversion efficiency. The plot also shows that the largest energy loss during combustion is due to heat transfer, which suggests that adding thermal barrier coatings to the cylinder can be considered to improve efficiency.

3.3 Combustion Phasing. Combustion timing and LTHR have a significant effect on RCCI combustion, as shown in previous

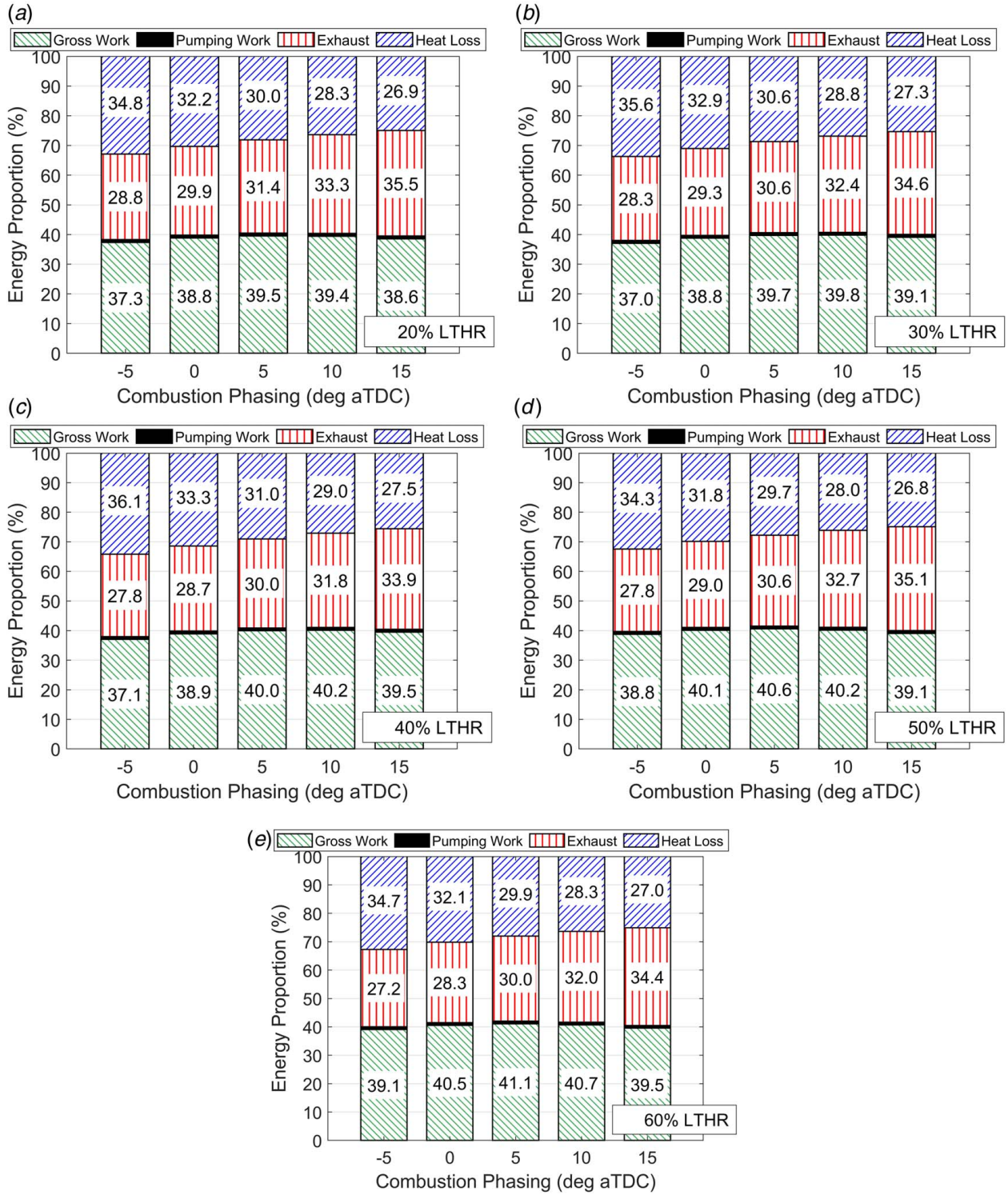

Fig. 11 Total engine system energy distribution as a function of combustion phasing for different LTHR fractions ranging from: (*a*) 20%, (*b*) 30%, (*c*) 40%, (*d*) 50%, and (e) 60%

research by Hariharan et al. [32]. The LTHR is caused by diesel combustion and is controlled by the reactivity difference between the low reactivity fuel (reformate) and the high reactivity fuel (diesel). The sensitivity of the combustion phasing to reactivity increases with the difference in reactivity. An analysis of fuel conversion efficiency and energy distribution with respect to combustion phasing (varying from −5 to 15 CAD after the top dead center (aTDC)) is performed in this section to find the optimal timing of the combustion phasing to achieve the highest fuel conversion efficiency for different LTHR fractions. In contrast with the study of LTHR fraction in the previous section, the crank angle of the start and end of combustion is varied to match the combustion phasing. The combustion phasing is defined as crank angle corresponding to 50% of total fuel mass burned (CA50), which is defined as the crank angle where 50% of total fuel mass has been burned. Figure 10 demonstrates the gross fuel conversion efficiency with respect to combustion phasing, and Fig. 11 illustrates the energy distribution with respect to the combustion phasing, with (a)–(e) referring to the LTHR fraction increased from 20% to 60%, respectively. Thus, the gross fuel conversion efficiency at LTHR of 20% increases from −5 to 5 CAD aTDC, reaches its peak value of 39.5%, and then decreases from 5 to 15 CAD aTDC. Similar trends appear at LTHR of 50–60%, where the gross fuel conversion efficiency increases from −5 to 5 CAD aTDC, and then decreases from 5 to 15 CAD aTDC. However, the gross fuel conversion efficiency for LTHR fraction between 30% and 40% has a slightly different trend, with all the cases reaching their maximum at around 10 CAD aTDC. Overall, the maximum fuel conversion efficiency is 41.1%, occurring for a 60% LTHR fraction and a CA50 at 5 CAD aTDC.

As the combustion phasing is retarded, more combustion occurs close to and after TDC. At close to TDC and during the expansion stroke, the piston is moving in the same direction as the expanding and burning fuel–air mixture. This reduces energy loss and, therefore, increases the gross work, as shown in Fig. 11. If the combustion phasing is retarded further, more of the combustion process occurs later in the expansion stroke and far away from TDC. Hence, the cylinder pressure and temperature are both reduced in magnitude, which reduces reaction rates and the fraction of fuel burned, thus causing a reduction of gross work and a decrease in gross fuel conversion efficiency. Previous RCCI research by Ma et al. [54] using gasoline/diesel dual-fuel combustion showed that indicated specific fuel consumption decreased with retarding CA50 until it reached a minimum value and then increased as CA50 was further retarded. An investigation by Mohammadian et al. [55] with single-fuel RCCI using isobutanol and DTBP additive also showed a decrease of indicated fuel conversion efficiency when the major combustion period was close to TDC, which is similar to the results shown in Fig. 10. The pumping work is almost constant with respect to the combustion phasing and LTHR fraction. The energy contained in exhaust gas monotonically increased with respect to the combustion phasing from 28.8% to 35.5% with 20% LTHR and from 27.2% to 34.4% with 60% LTHR. The exhaust energy is affected by the temperature of exhaust gas and the fraction of unburned fuel. Since the cylinder temperature decreases at early expansion stroke and increases at late expansion stroke, the increase of energy in the exhaust gas is due to the effect of cylinder temperature at late expansion stroke, with the bulk of the reactions occurring after TDC. The heat loss to the cylinder wall is monotonically decreasing with respect to the combustion phasing from 34.8% to 26.9% with 20% LTHR and from 34.7% to 27% with 60% LTHR, which is due to the decreasing of temperature at early expansion stroke and corresponded decreasing of heat transfer coefficient.

By comparing Fig. 10 to Fig. 8, it is evident that the gross fuel conversion efficiency decreases with increasing LTHR at the advanced combustion phasing cases. Conversely, at retarded combustion phasing, gross fuel conversion efficiency increases as the fraction of LTHR is increasing. This is due to more of the combustion process occurring after TDC, thus maximizing gross work. The fuel conversion efficiency achieved in this study is higher than the experimental result shown by Hariharan et al. [32]. This suggests that the modified combustion profile, with delayed combustion phasing close to TDC and a high LTHR fraction, can yield a higher fuel conversion efficiency. This strategy can be used as a potential target for RCCI combustion in future studies.

4 Conclusions

In this paper, a SWF and two DWFs were estimated to predict the MFB curve using experimental data collected from single-fuel RCCI combustion. The DWF with the highest accuracy was selected for further combustion analysis using a 1D thermodynamic model built on GT-POWER. A modeling study of the fraction of LTHR and combustion phasing was performed and the fuel conversion efficiency and energy distribution were investigated using this 1D model. From a detailed analysis of the DWF and the thermodynamic simulation results, the following conclusions can be drawn:

- The DDWF is able to predict the MFB profile for single-fuel RCCI combustion and it fits the best experimental data. The RDWF predicts a similar MFB profile as the DDWF. The SWF is not able to provide a combustion profile with high accuracy.
- The LTHR has an effect on fuel conversion efficiency and heat loss. At the advanced combustion phasing, the indicated net fuel conversion efficiency monotonically decreases from 37.5% to 35.2% as the fraction of LTHR is increased. The exhaust energy is decreased from 26.9% to 24.2% and the heat loss to the cylinder wall increases from 34.7% to 39.7% as the LTHR fraction is increasing.
- The indicated fuel conversion efficiency increases first and then decreases as the combustion phasing is retarded from before TDC to after TDC for different LTHR fractions. With a retarded combustion phasing, the indicated net fuel conversion efficiency increases as the fraction of LTHR is increased. The maximum efficiency of 41.1% is reached for LTHR of 60% and with CA50 at 5 CAD aTDC and 60%. The modified combustion profile with delayed CA50 and high LTHR fraction shows a potential combustion strategy that could achieve higher efficiency than previously demonstrated for single-fuel RCCI combustion.
- The exhaust gas energy monotonically increases as the combustion phasing is delayed. The maximum fraction of exhaust gas energy is 35.5% with CA50 occurring at −5 aTDC and for 20% LTHR, while the minimum is 33.9% with CA50 at 15 aTDC and for 40% LTHR. The energy loss to the cylinder wall decreases as the combustion phasing is retarded. The maximum fraction of heat loss is 36.1% with CA50 −5 aTDC and 40% LTHR and the minimum is 26.8% with CA50 at 15 aTDC and with 50% LTHR.

Ultimately, this study numerically determines the most appropriate LTHR fraction and combustion profile to achieve the maximum efficiency for single-fuel RCCI combustion for the conditions studied. In addition, these findings can be utilized to alter the reformate fuel catalyzing process to develop a reformate fuel composition that can deliver the desired LTHR percentage, thus unlocking the most favorable performance possible for single-fuel RCCI combustion.

Acknowledgment

The authors would like to acknowledge the financial support of the Department of Energy (DOE), provided through award number DE-EE0007216 to perform this research. The authors also appreciate the contributions of Professor Benjamin Lawler and Dr. Deivanayagam Hariharan for providing a portion of the experimental data.

References

[1] Johnson, T. V., 2009, "Review of Diesel Emissions and Control," Int. J. Engine Res., **10**(5), pp. 275–285.
[2] Noguchi, M., Tanaka, Y., Tanaka, T., and Takeuchi, Y., 1979, "A Study on Gasoline Engine Combustion by Observation of Intermediate Reactive Products During Combustion," SAE Technical Paper Series, SAE International.
[3] Onishi, S., Jo, S. H., Shoda, K., Jo, P. D., and Kato, S., 1979, "Active Thermo-Atmosphere Combustion (ATAC)—A New Combustion Process for Internal Combustion Engines," SAE Technical Paper.
[4] Najt, P. M., and Foster, D. E., 1983, "Compression-Ignited Homogeneous Charge Combustion," SAE Technical Paper.
[5] Kimura, S., Aoki, O., Ogawa, H., Muranaka, S., and Enomoto, Y., 1999, "New Combustion Concept for Ultra-Clean and High-Efficiency Small Di Diesel Engines," SAE Technical Paper.
[6] Zhao, F., Asmus, T. N., Assanis, D. N., Dec, J. E., Eng, J. A., and Najt, P. M., 2003, "Homogeneous Charge Compression Ignition (HCCI) Engines," SAE Technical Paper.
[7] Tanaka, S., Ayala, F., and Keck, J. C., 2003, "A Reduced Chemical Kinetic Model for HCCI Combustion of Primary Reference Fuels in a Rapid Compression Machine," Combust. Flame, **133**(4), pp. 467–481.
[8] Soyhan, H. S., Mauss, F., and Sorusbay, C., 2002, "Chemical Kinetic Modeling of Combustion in Internal Combustion Engines Using Reduced Chemistry," Combust. Sci. Technol., **174**(11–12), pp. 73–91.
[9] Genzale, C. L., Reitz, R. D., and Musculus, M. P., 2009, "Effects of Piston Bowl Geometry on Mixture Development and Late-Injection Low-Temperature Combustion in a Heavy-Duty Diesel Engine," SAE Int. J. Engines, **1**(1), pp. 913–937.
[10] Bobba, M., Musculus, M., and Neel, W., 2010, "Effect of Post Injections on In-Cylinder and Exhaust Soot for Low-Temperature Combustion in a Heavy-Duty Diesel Engine," SAE Int. J. Engines, **3**(1), pp. 496–516.
[11] Cao, L., Bhave, A., Su, H., Mosbach, S., Kraft, M., Dris, A., and McDavid, R. M., 2009, "Influence of Injection Timing and Piston Bowl Geometry on PCCI Combustion and Emissions," SAE Int. J. Engines, **2**(1), pp. 1019–1033.
[12] Bessonette, P. W., Schleyer, C. H., Duffy, K. P., Hardy, W. L., and Liechty, M. P., 2007, "Effects of Fuel Property Changes on Heavy-Duty HCCI Combustion," SAE Technical Paper.
[13] Inagaki, K., Fuyuto, T., Nishikawa, K., Nakakita, K., and Sakata, I., 2006, "Dual-Fuel PCI Combustion Controlled by In-Cylinder Stratification of Ignitability," SAE Technical Paper.
[14] Kokjohn, S. L., Hanson, R. M., Splitter, D. A., and Reitz, R. D., 2010, "Experiments and Modeling of Dual-Fuel HCCI and PCCI Combustion Using In-Cylinder Fuel Blending," SAE Int. J. Engines, **2**(2), pp. 24–39.
[15] Dempsey, A. B., Ryan Walker, N., Gingrich, E., and Reitz, R. D., 2014, "Comparison of Low Temperature Combustion Strategies for Advanced Compression Ignition Engines With a Focus on Controllability," Combust. Sci. Technol., **186**(2), pp. 210–241.
[16] Kokjohn, S. L., Hanson, R. M., Splitter, D. A., and Reitz, R. D., 2011, "Fuel Reactivity Controlled Compression Ignition (RCCI): A Pathway to Controlled High-Efficiency Clean Combustion," Int. J. Engine Res., **12**(3), pp. 209–226.
[17] Hanson, R. M., Kokjohn, S. L., Splitter, D. A., and Reitz, R. D., 2010, "An Experimental Investigation of Fuel Reactivity Controlled PCCI Combustion in a Heavy-Duty Engine," SAE Int. J. Engines, **3**(1), pp. 700–716.
[18] Ryan Walker, N., Wissink, M. L., DelVescovo, D. A., and Reitz, R. D., 2015, "Natural Gas for High Load Dual-Fuel Reactivity Controlled Compression Ignition in Heavy-Duty Engines," ASME J. Energy Resour. Technol., **137**(4), p. 042202.
[19] Reitz, R. D., and Duraisamy, G., 2015, "Review of High Efficiency and Clean Reactivity Controlled Compression Ignition (RCCI) Combustion in Internal Combustion Engines," Prog. Energy Combust. Sci., **46**, pp. 12–71.
[20] Paykani, A., Kakaee, A.-H., Rahnama, P., and Reitz, R. D., 2016, "Progress and Recent Trends in Reactivity-Controlled Compression Ignition Engines," Int. J. Eng. Res., **17**(5), pp. 481–524.
[21] Splitter, D., Hanson, R., Kokjohn, S., and Reitz, R. D., 2011, "Reactivity Controlled Compression Ignition (RCCI) Heavy-Duty Engine Operation at Mid- and High-Loads With Conventional and Alternative Fuels," SAE Technical Paper.
[22] Kaddatz, J., Andrie, M., Reitz, R. D., and Kokjohn, S., 2012, "Light-Duty Reactivity Controlled Compression Ignition Combustion Using a Cetane Improver," SAE Technical Paper.
[23] Dempsey, A. B., Ryan Walker, N., and Reitz, R., 2013, "Effect of Cetane Improvers on Gasoline, Ethanol, and Methanol Reactivity and the Implications for RCCI Combustion," SAE Int. J. Fuels Lubr., **6**(1), pp. 170–187.
[24] Splitter, D., Reitz, R., and Hanson, R., 2010, "High Efficiency, Low Emissions RCCI Combustion by Use of a Fuel Additive," SAE Int. J. Fuels Lubr., **3**(2), pp. 742–756.
[25] Lawler, B., and Mamalis, S., 2018, "Single-Fuel Reactivity Controlled Compression Ignition Combustion Enabled by Onboard Fuel Reformation," US Patent Ap. 15/082,469.
[26] Chuahy, F. D., and Kokjohn, S. L., 2017, "Effects of Reformed Fuel Composition in 'Single' Fuel Reactivity Controlled Compression Ignition Combustion," Appl. Energy, **208**, pp. 1–11.
[27] Ran, Z., Longtin, J., and Assanis, D., 2021, "Investigating Anode Off-Gas Under Spark-Ignition Combustion for SOFC-Ice Hybrid Systems," Int. J. Engine Res.
[28] Ran, Z., Assanis, D., Hariharan, D., and Mamalis, S., 2020, "Experimental Study of Spark-Ignition Combustion Using the Anode Off-Gas From a Solid Oxide Fuel Cell," SAE Technical Paper.
[29] Nikiforakis, I., Ran, Z., Sprengel, M., Brackett, J., Babbit, G., and Assanis, D., 2021, "Investigating Realistic Anode Off-Gas Combustion in Sofc/Ice Hybrid Systems: Mini Review and Experimental Evaluation," Int. J. Engine Res.
[30] Hariharan, D., Yang, R., Zhou, Y., Gainey, B., Mamalis, S., Smith, R. E., Lugo-Pimentel, M. A., et al., 2019, "Catalytic Partial Oxidation Reformation of Diesel, Gasoline, and Natural Gas for Use in Low Temperature Combustion Engines," Fuel, **246**, pp. 295–307.
[31] Yang, R., Hariharan, D., Zilg, S., Mamalis, S., and Lawler, B., 2018, "Efficiency and Emissions Characteristics of an HCCI Engine Fueled by Primary Reference Fuels," SAE Int. J. Engines, **11**(6), pp. 993–1006.
[32] Hariharan, D., Gainey, B., Yan, Z., Mamalis, S., and Lawler, B., 2020, "Experimental Study of the Effect of Start of Injection and Blend Ratio on Single Fuel Reformate RCCI," ASME J. Eng. Gas Turbines Power, **142**(8), p. 081010.
[33] Guleria, G., Lopez-Pintor, D., Dec, J. E., and Assanis, D., 2021, "A Comparative Study of Gasoline Skeletal Mechanisms Under Partial Fuel Stratification Conditions Using Large Eddy Simulations," Int. J. Engine Res.
[34] Heywood, J. B., 1988, *Internal Combustion Engine Fundamentals*, Vol. 930, McGraw-Hill, New York.
[35] Zheng, J., and Caton, J. A., 2012, "Use of a Single-Zone Thermodynamic Model With Detailed Chemistry to Study a Natural Gas Fueled Homogeneous Charge Compression Ignition Engine," Energy Convers. Manage., **53**(1), pp. 298–304.
[36] Liu, Z., and Chen, R., 2009, "A Zero-Dimensional Combustion Model With Reduced Kinetics for SI Engine Knock Simulation," Combust. Sci. Technol., **181**(6), pp. 828–852.
[37] Neshat, E., and Saray, R. K., 2014, "Development of a New Multi Zone Model for Prediction of HCCI (Homogenous Charge Compression Ignition) Engine Combustion, Performance and Emission Characteristics," Energy, **73**, pp. 325–339.
[38] Yasar, H., Soyhan, H. S., Walmsley, H., Head, B., and Sorusbay, C., 2008, "Double-Wiebe Function: An Approach for Single-Zone HCCI Engine Modeling," Appl. Therm. Eng., **28**(11–12), pp. 1284–1290.
[39] Stone, R., 1999, *Introduction to Internal Combustion Engines*, Vol. 3, Springer, New York.
[40] Assanis, D., Karvounis, E., Sekar, R., and Marr, W., 1993, "Heat Release Analysis of Oxygen-Enriched Diesel Combustion," ASME J. Eng. Gas Turbines Power, **115**(4), pp. 761–768.
[41] Yeliana, Y., Cooney, C., Worm, J., Michalek, D., and Naber, J., 2008, "Wiebe Function Parameter Determination for Mass Fraction Burn Calculation in an Ethanol-Gasoline Fuelled SI Engine," J. KONES, **15**(3), pp. 567–574.
[42] Yeliana, Y., Cooney, C., Worm, J., Michalek, D. J., and Naber, J. D., 2011, "Estimation of Double-Wiebe Function Parameters Using Least Square Method for Burn Durations of Ethanol-Gasoline Blends in Spark Ignition Engine Over Variable Compression Ratios and EGR Levels," Appl. Therm. Eng., **31**(14–15), pp. 2213–2220.
[43] Lindström, F., Ångström, H.-E., Kalghatgi, G., and Möller, C. E., 2005, "An Empirical SI Combustion Model Using Laminar Burning Velocity Correlations," SAE Trans., **114**(4), pp. 833–846.
[44] Yıldız, M., and Albayrak Çeper, B., 2017, "Zero-Dimensional Single Zone Engine Modeling of an SI Engine Fuelled With Methane and Methane-Hydrogen Blend Using Single and Double Wiebe Function: A Comparative Study," Int. J. Hydrogen Energy, **42**(40), pp. 25756–25765.
[45] Liu, J., and Dumitrescu, C. E., 2019, "Single and Double Wiebe Function Combustion Model for a Heavy-Duty Diesel Engine Retrofitted to Natural-Gas Spark-Ignition," Appl. Energy, **248**, pp. 95–103.
[46] Liu, J., and Dumitrescu, C. E., 2020, "Improved Thermodynamic Model for Lean Natural Gas Spark Ignition in a Diesel Engine Using a Triple Wiebe Function," ASME J. Energy Resour. Technol., **142**(6), p. 062303.
[47] Liu, J., Ulishney, C., and Dumitrescu, C. E., 2020, "Characterizing Two-Stage Combustion Process in a Natural Gas Spark Ignition Engine Based on Multi-Wiebe Function Model," ASME J. Energy Resour. Technol., **142**(10), p. 102302.
[48] Awad, S., Varuvel, E. G., Loubar, K., and Tazerout, M., 2013, "Single Zone Combustion Modeling of Biodiesel From Wastes in Diesel Engine," Fuel, **106**, pp. 558–568.
[49] Yang, R., Ran, Z., and Assanis, D., 2021, "Estimation of Wiebe Function Parameters for Syngas and Anode Off-Gas Combustion in Spark-Ignition Engines," Paper Presented at the Internal Combustion Engine Division Fall Technical Conference, Virtual, Online, Oct. 13–15.
[50] Ran, Z., Hadlich, R. R., Yang, R., Dayton, D. C., Mante, O. D., and Assanis, D., 2022, "Experimental Investigation of Naphthenic Biofuel Surrogate Combustion in a Compression Ignition Engine," Fuel, **312**, p. 122868.
[51] Hohenberg, G. F., 1979, "Advanced Approaches for Heat Transfer Calculations," SAE Technical Paper.
[52] Gamma Technologies Inc, 2017, GT-POWER User's Manual. "Gt-Suite Version 2016."
[53] Wang, Y., Yao, M., Li, T., Zhang, W., and Zheng, Z., 2016, "A Parametric Study for Enabling Reactivity Controlled Compression Ignition (RCCI) Operation in Diesel Engines at Various Engine Loads," Appl. Energy, **175**, pp. 389–402.
[54] Ma, S., Zheng, Z., Liu, H., Zhang, Q., and Yao, M., 2013, "Experimental Investigation of the Effects of Diesel Injection Strategy on Gasoline/Diesel Dual-Fuel Combustion," Appl. Energy, **109**, pp. 202–212.
[55] Mohammadian, A., Chehrmonavari, H., Kakaee, A., and Paykani, A., 2020, "Effect of Injection Strategies on a Single-Fuel RCCI Combustion Fueled With Isobutanol/Isobutanol+ DTBP Blends," Fuel, **278**, p. 118219.